Symmetry-resolved x-ray absorption fine structure and resonant Auger-spectator-electron decay study of O $1s \rightarrow$ Rydberg resonances in O_2

T. Tanaka,[1] R. Feifel,[2,3] M. Kitajima,[1] H. Tanaka,[1] S. L. Sorensen,[4] R. Sankari,[5] A. De Fanis,[3] M.-N. Piancastelli,[2,6] L. Karlsson,[2] and K. Ueda[3,*]

[1]*Department of Physics, Sophia University, Tokyo 102-8554, Japan*

[2]*Department of Physics, Uppsala University, Box 530, SE-751 21 Uppsala, Sweden*

[3]*Institute of Multidisciplinary Research for Advanced Materials, Tohoku University, Sendai 980-8577, Japan*

[4]*Department of Synchrotron Radiation Research, Institute of Physics, University of Lund, Box 118, S-221 00 Lund, Sweden*

[5]*Department of Physical Sciences, University of Oulu, P.O. Box 3000, 90014, Finland*

[6]*Department of Chemical Sciences and Technologies and INFM, University "Tor Vergata," I-00133 Rome, Italy*

(Received 4 July 2008; published 29 August 2008)

A series of resonant Auger-electron spectra excited at selected photon energies across the O $1s \rightarrow$ Rydberg resonances in O_2 has been measured. Applying a spectator-electron shake relaxation model originally introduced for atomic resonant Auger-electron spectra, and using, to a large extent, the assignments for the core-excited resonances available from the literature, many of the observed spectator Auger-electron final states are assigned in terms of cationic Rydberg series. Vice versa the resonant Auger-electron spectra are used for consistency tests of the literature assignments for the core-excited intermediate Rydberg states. For some of the latter, alternative assignments are proposed for reasons discussed.

DOI: 10.1103/PhysRevA.78.022516 PACS number(s): 33.70.Ca, 33.80.Eh, 34.50.Gb

I. INTRODUCTION

Resonant Auger-electron spectroscopy, where the projection of the excited neutral intermediate state onto final one- and two-hole states is monitored, is known to be a sensitive tool to investigate complex inner-valence spectral features [1–5]. This method is inherently interconnected with the knowledge of the involved core-excited states, and can provide important insights on those.

The soft x-ray absorption spectrum of molecular oxygen near the O $1s$ threshold has been the subject of great interest for many years (see, e.g., Refs. [6–19], and references therein). Whereas the O $1s \rightarrow \pi^*$ resonance, located at ~530.8 eV photon energy, reflects a comparatively simple vibrational fine structure [21], the region between ~535 and ~545 eV is much more complex due to the presence of broad sigma resonances and discrete states converging to the $^4\Sigma_u^-$ and $^2\Sigma_u^-$ core-hole states at 543.39(5) and 544.43(5) eV [20], respectively. Several of the previous investigations illustrate the difficulty of unambiguously identifying the resonances in this spectral region. The open-shell nature of the oxygen molecule substantially complicates the interpretation of the spectra, and the difficulty of calculating these core-excited states is amplified. In particular, the O $1s \rightarrow \sigma^*$ resonances received quite a lot of attention over the years, due to an early controversy concerning the energy splitting between the quartet and doublet states [7–14]. However, these difficulties seem to be resolved now in a recent investigation which built on the combination of photoabsorption, constant ionic state experiments, and extensive configuration interaction calculations [16].

Also, the discrete resonant states have been investigated in several previous studies, where, in particular, the symmetry-resolved photoabsorption studies of Kosugi and co-workers in combination with high-level *ab initio* calculations [10,13,19] constitute one of the most detailed investigations of this part of the oxygen $1s$ near-edge absorption spectrum. In some investigations [11,15] x-ray absorption spectroscopy of O_2 was accompanied by resonant Auger-electron spectroscopy, where the latter has partially been used as a "fingerprint" method for monitoring the core-excited states [11]. In both the work of Neeb *et al.* [11] and Kivimäki *et al.* [15] it was already realized that the resonant Auger-electron spectra measured for high Rydberg excitations closely resemble the normal Auger-electron spectrum [22], however, no attempts were made to assign the spectral features in the resonantly excited electron spectra.

Very recently, we presented a study [23] of two-resonant-electron spectra of O_2 measured on top of the 541.80 and 541.97 eV absorption lines, where we utilized a relaxation model [24] to interpret the singly ionized final states. The model implied a spectator electron in a Rydberg state, where the series converges to a doubly ionized electronic state which is known from normal Auger-electron spectroscopy [22]. Briefly, the resonant Auger-electron spectra were considered as the sum of normal Auger-electron spectra, all associated with, in a simplified picture, the $(O\ 1s)^{-1}\ ^4\Sigma_u^-$ intermediate core hole state, shifted by the screening energy for the given Rydberg state, and with intensities modified by the transition integrals.

In this work we elaborate on this first investigation by examining a series of resonant Auger-electron spectra excited at ten selected photon energies across the O $1s \rightarrow$ Rydberg resonances in O_2. Applying the relaxation model on the grounds of assignments for the core-excited resonances known from the literature [10,13,19], many of the observed spectator-Auger-electron final states will be assigned in terms of cationic Rydberg series, and the resonant Auger-electron spectra are used for consistency tests of the

*ueda@tagen.tohoku.ac.jp

literature assignments available for the core-excited intermediate Rydberg states.

II. EXPERIMENTAL DETAILS

The experiments were carried out at the undulator beamline 27SU at SPring-8, Japan, which is equipped with a high-resolution soft x-ray monochromator [25,26]. The radiation source is a figure-eight undulator which can provide either horizontally or vertically linear polarized light by setting the undulator gap appropriately [27,28]. The electron spectra were recorded using a high-resolution hemishperical electron-energy analyzer (Gammadata Scienta SES-2002) fitted with a gas cell. The lens axis of the electron spectrometer is in the horizontal direction, at right angles to the photon beam direction [29]. In this arrangement, electron spectra recorded with horizontal and vertical polarization correspond to the electron emission parallel (0°) and perpendicular (90°) to the $\mathcal{E}$ vector, respectively. The monitor of the photon flux for the normalization is made by two drain currents on the last refocusing mirror and after the gas sample. All electron spectra are normalized to the data acquisition time, the gas pressure, and the photon flux. Spectra corrected for anisotropic electron emission can then be constructed by combining the 0° and 90° spectra measured at the same photon energy according to the following equation which assumes 100% linear polarization:

$$I(54.7^\circ) = I(0^\circ) + 2\,I(90^\circ). \quad (1)$$

Spectra of this type will be referred to as "magic angle" (54.7°) spectra in the following. The degree of linear polarization was measured by studying the Ne 2*s* and 2*p* photolines, and was found to be larger than 0.98 for the current optical settings [30], which justifies the assumption that all photons are completely linear polarized. The monochromator band pass was set to 70 meV full width at half maximum (FWHM), the electron spectrometer band pass to 63 meV, and the inhomogeneous Doppler broadening due to thermal motion of the sample molecules is estimated to be around 50 meV, resulting in a total experimental linewidth for the electron spectra of around 110 meV. Electron spectra were recorded at various selected photon energies across the O $1s \rightarrow$ Rydberg resonances and well above the ionization threshold at 650 eV.

The photon energy calibration was made by measuring the total ion yield (TIY) using a 4π-sr time-of-flight (TOF) ion detector installed in the general purpose experimental chamber, placed between the monochromator and the electron spectrometer, and comparing to published absorption spectra [21,31]. The photon energy determination is found to be accurate to within ± 40 meV. In order to obtain symmetry-resolved near-edge x-ray absorption fine structure spectra, we used two identical ion detectors mounted at 0° and 90° with respect to the $\mathcal{E}$ vector [32] and located 250 mm downstream from the TIY detector, to each of which a retarding potential of 6 V has been applied for detecting ions with kinetic energies higher than 6 eV. For recording the TIY and symmetry-resolved absorption spectra presented below, the monochromator bandwidth was set to around 30 meV. Also, these spectra are normalized to the data acquisition time, the gas pressure, and the photon flux. The resonant Auger-electron spectra were calibrated using the $c\,^4\Sigma_u^-(v=0)$ state binding energy of 24.564 eV as internal reference [33]. This line is well defined and therefore well suited for calibration purposes. For the normal Auger spectrum we used the kinetic energies from Larsson *et al.* [22]. O_2 gas was commercially obtained with a stated purity of >99.99%.

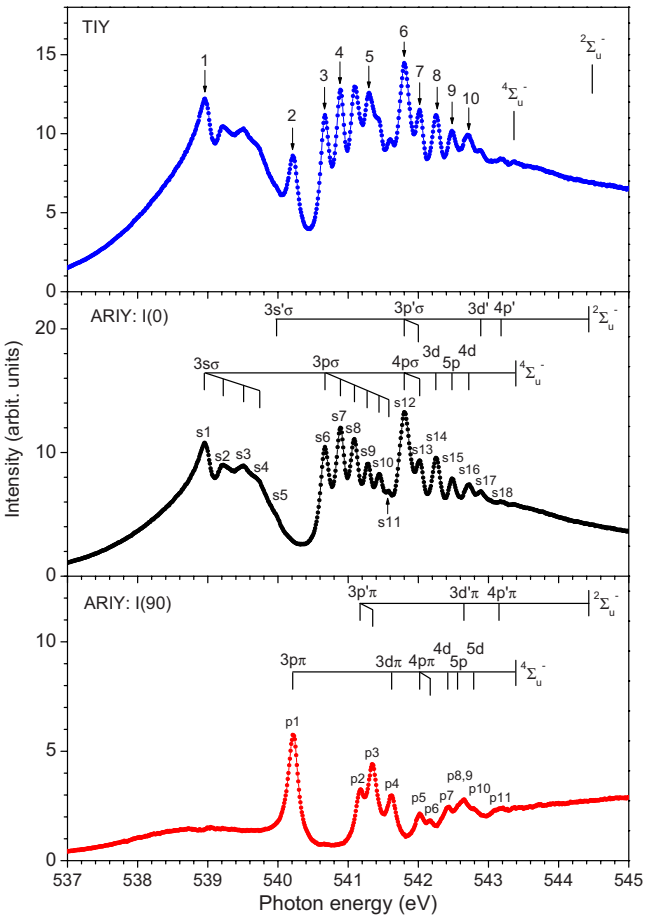

FIG. 1. (Color online) Upper panel: high-resolution *K*-edge total ion yield near-edge x-ray absorption fine structure spectrum of O_2 recorded in the photon energy range between 537 and 545 eV. The photon energies used for recording a series of resonant Auger-electron spectra are numbered 1–10. Middle panel: high-resolution symmetry-resolved $\Delta\Lambda=0$ (Σ channel) ion yield spectrum including assignments as discussed in the text and summarized in Table I. Lower panel: high-resolution symmetry-resolved $\Delta\Lambda=1$ (Π channel) ion yield spectrum including assignments as discussed in the text and summarized in Table II.

III. RESULTS AND DISCUSSION

In Fig. 1 we present *K*-edge x-ray absorption spectra of O_2 recorded in the photon energy range between 537 and 545 eV. The top panel contains a total ion yield spectrum which shows more detail than our earlier work [23] due to superior resolution. The energies used for the recording of the resonant Auger-electron spectra to be discussed below,

TABLE I. Σ-channel Rydberg assignments for O_2 in the O 1*s* core excitation region.

Peak	$h\nu$ (eV)	Assignment		ν (meV)	n^*	
		$^4\Sigma_u^-$	$^2\Sigma_u^-$		$^4\Sigma_u^-$	$^2\Sigma_u^-$
s1	538.95	$3s\sigma$			1.75	
s2	539.22	$3s\sigma$ $\nu=1$		270		
s3	539.50	$3s\sigma$ $\nu=2$		280		
s4	539.74	$3s\sigma$ $\nu=3$		240		
s5	539.98		$3s'\sigma$			1.75
s6	540.67	$3p\sigma$			2.24	
s7	540.89	$3p\sigma$ $\nu=1$		220		
s8	541.09	$3p\sigma$ $\nu=2$		200		
s9	541.28	$3p\sigma$ $\nu=3$		190		
s10	541.44	$3p\sigma$ $\nu=4$		160		
s11	541.58	$3p\sigma$ $\nu=5$		140		
s12	541.80	$4p\sigma$	$3p'\sigma$		2.93	2.27
s13	542.02	$4p\sigma$ $\nu=1$	$3p'\sigma$ $\nu=1$	220		
s14	542.25	$3d\sigma$			3.45	
s15	542.48	$5p\sigma+3d\sigma$ $\nu=1$		230		
s16	542.72	$4d\sigma$			4.51	
s17	542.89		$3d'\sigma$			2.97
s18	543.18		$4p'\sigma$?			3.30
	543.39	I.P.				
	544.43		I.P			

and the two O 1*s* ionization thresholds $^4\Sigma_u^-$ and $^2\Sigma_u^-$ at 543.39 and 544.43 eV [20], are marked in this figure. The lower two panels contain high-resolution symmetry-resolved ion-yield spectra measured at 0° and 90° which correspond to $\Delta\Lambda=0$ [Σ channels; $I(0°)$] and $\Delta\Lambda=1$ [Π channels; $I(90°)$] transitions. Assignments are also included in this figure which are summarized in Tables I and II, and which we shall come back to (Rydberg series converging to the $^2\Sigma_u^-$ ionization limit are marked with a prime in distinction to the Rydberg series converging to the $^4\Sigma_u^-$ ionization limit following the notation of Ref. [13]). Similar spectra have been reported earlier at somewhat lower energy resolution, together with *ab initio* potential curve calculations and assignments (see Refs. [10,13,19]).

As part of the resonant Auger-electron spectra to be examined, we presented recently in some detail [23] the ones

TABLE II. Π-channel Rydberg assignments for O_2 in the O 1*s* core excitation region.

Peak	$h\nu$ (eV)	Assignment		ν (meV)	n^*	
		$^4\Sigma_u^-$	$^2\Sigma_u^-$		$^4\Sigma_u^-$	$^2\Sigma_u^-$
p1	540.22	$3p\pi$			2.07	
p2	541.18		$3p'\pi$			2.05
p3	541.34		$3p'\pi$ $\nu=1$	160		
p4	541.62	$3d\pi$			2.77	
p5	542.02	$4p\pi$			3.15	
p6	542.17	$4p\pi$ $\nu=1$		150		
p7	542.42	$4d\pi$			3.75	
p8	542.56	$5p\pi$			4.05	
p9	542.65		$3d'\pi$			2.76
p10	542.79	$5d\pi$			4.76	
p11	543.16		$4p'\pi$			3.27
	543.39	I.P.				
	544.43		I.P.			

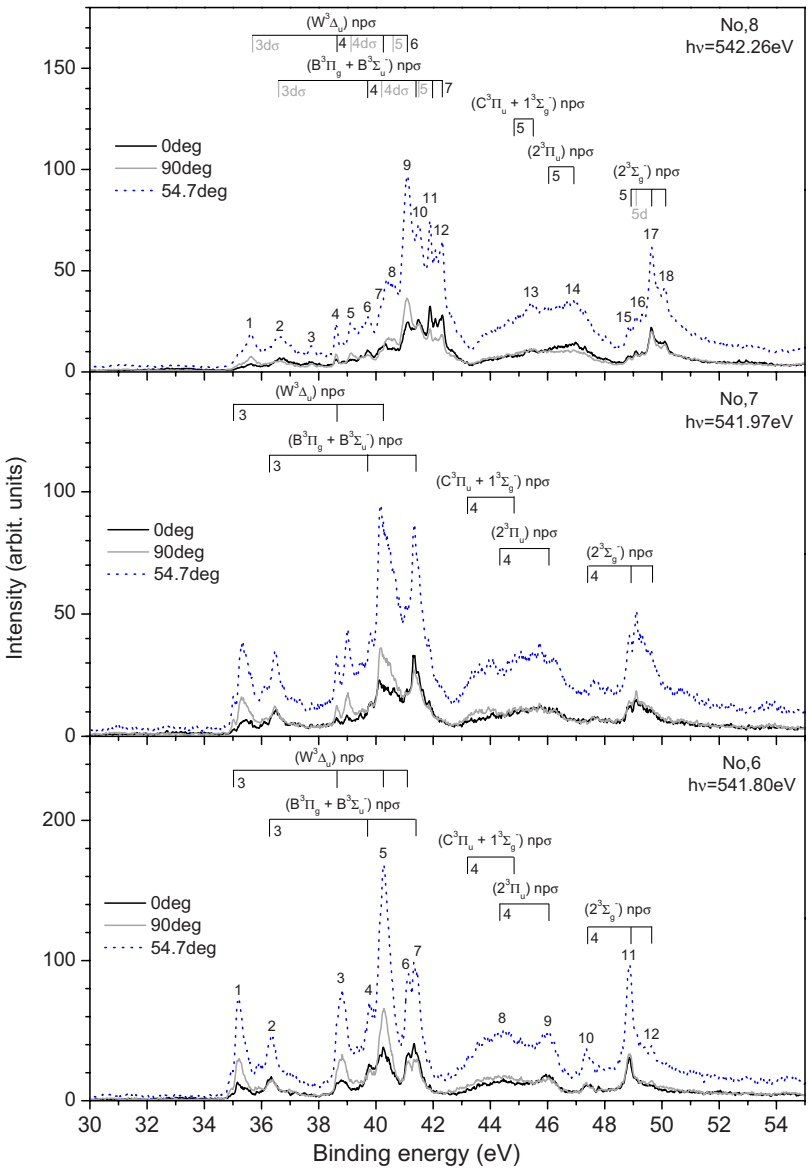

FIG. 2. (Color online) Normalized resonant Auger-electron spectra of O_2 obtained for the photon energies 541.80 eV (lower panel), 541.97 eV (middle panel), and 542.26 eV (upper panel), respectively. Spectra recorded at 0° and 90° relative to the electric field vector of the linearly polarized synchrotron light are included, as well as the ones corrected for anisotropic electron emission (54.7°). Assignments of the various spectator Auger-electron final states in terms of Rydberg series in the cation converging towards the dicationic ionization limits are also included together with the principal quantum number n for some of the states (see also Table III).

corresponding to the excitations on top of peaks 6 and 7 of Fig. 1 ($h\nu$=541.80 and 541.97 eV photon energy), respectively, both for the angles of 0° and 54.7° relative to the electric field vector of the linear polarized synchrotron light. These spectra are displayed together with the previously unpublished 90° recordings in the lower and middle panel of Fig. 2. The assignments of various Auger-electron final states in terms of Rydberg series, as made for these spectra in our preceding work [23] based on the results of previous experiments and theoretical investigations [6–19,22], are also included, and we shall briefly recapitulate how they were obtained.

The resonant Auger-electron spectra are composed of two distinct sets of spectral features. The low energy part between ~10 and ~35 eV binding energy (not displayed here; see, e.g., Ref. [34]) closely resembles the direct photoionization spectrum, while the higher binding energy region (above 35 eV) belongs primarily to spectator (two-hole, one-particle) final states. Since the spectra recorded on top of peaks 6 and 7 of Fig. 1 ($h\nu$=541.80 and 541.97 eV, respectively) owe, above 35 eV binding energy, some apparently strong similarities to the ordinary Auger-electron spectrum recorded at 650 eV, as exemplarily shown in Fig. 3 for the electron spectrum 6 ($h\nu$=541.80 eV), an interpretation of the spectator-Auger-electron final states was made in terms of a series of Rydberg states in the cation converging towards the dicationic ionization limits, where we treated the quantum defect as a parameter. This interpretation is based on the use of a relaxation model introduced earlier for atomic resonant Auger-electron spectra [24], and which corresponds to the Manne-Åberg model [35] known from conventional core-level photoelectron spectroscopy. To begin with, the assignments of the resonant Auger-electron spectra assumed that the $d\sigma$ and $d\pi$ ionic Rydberg states are small, and that the relevant intermediate neutral states at peaks 6 and 7 in Fig. 1 (541.80 and 541.97 eV) governing the Auger decay are essentially the $v=0$ and 1 vibrational components of the O $1s^{-1}$ ($^4\Sigma_u^-$) $4p\sigma$ Rydberg state. Here we neglected possible contributions from the O $1s^{-1}$ ($^2\Sigma_u^-$) $3p'\sigma$ Rydberg state [10,13,19] and will return to this point later. To identify the Auger-

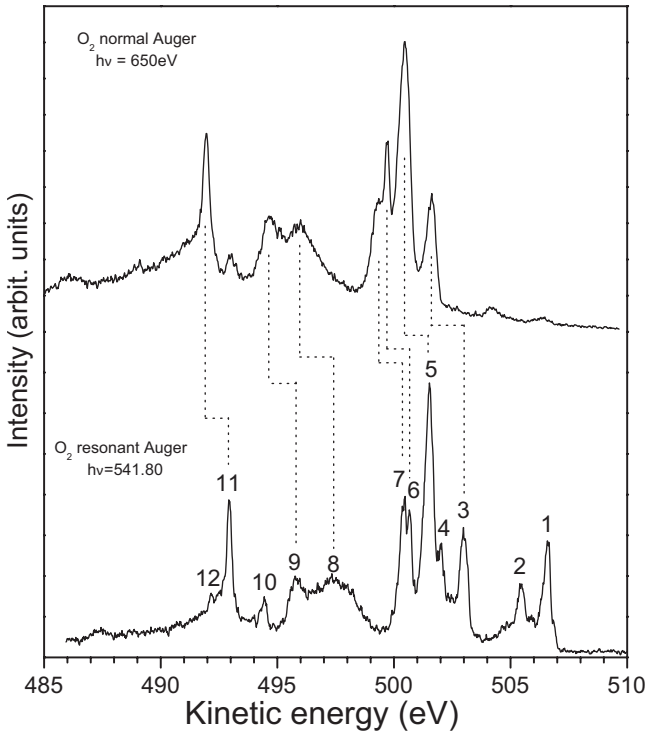

FIG. 3. The resonant Auger-electron spectrum recorded at the photon energy 541.80 eV and plotted on a kinetic energy scale in comparison to the normal Auger-electron spectrum obtained at the photon energy 650 eV.

electron final states, we assumed that the Auger lines belonging to the same Rydberg series have the same angular distribution of the emitted Auger electrons. For example, the similar angular distributions in the Rydberg series converging to the W $^3\Delta_u$ dicationic state, as marked in the resonant Auger-electron spectrum 6, illustrates this nicely. Based on these assumptions, a number of Auger-electron final Rydberg states could be identified as marked in Fig. 2 and which are summarized in Table III (for orientation we included also in this table the numbering of the states according to the normal Auger lines from Fig. 3).

Since we have information at hand both from the high-resolution resonant Auger-electron spectra and the high-resolution x-ray absorption fine structure spectra, we can perform "consistency tests" on the assignments made. For example, by comparing the electron spectra 6 and 7 in Fig. 2 ($h\nu$=541.80 and 541.97 eV), we noticed that the intensity ratios of the bands for the groups of different n in the spectator Auger-electron final states are the same. On the contrary, by comparing the electron spectra 6 and 8 (corresponding to 541.80 and 542.26 eV photon energy), as displayed in the lower and upper panels of Fig. 2, we find a clear difference in the spectral distribution. In particular, we can observe a sharp drop of intensity in the $4p\sigma$ final states of the electron spectrum 8 ($h\nu$=542.26 eV). This suggests that the difference between the 541.80 and 541.97 eV recordings (corresponding to peaks 6 and 7 of Fig. 1) is most likely not in the principal quantum number of the intermediate state but in the vibrational excitation which agrees well with parts of the assignment made by Kosugi and co-workers [10,13,19] for these resonance lines. It is worth noting that although the integrated intensities are the same when comparing various parts of the electron spectra 6 and 7 ($h\nu$=541.80 and 541.97 eV), the peak profiles differ to varying degrees. This behavior is expected as a result of differences in the Franck-Condon factors for transitions from the $v=0$ and $v=1$ intermediate states. Furthermore, as can be seen from the electron spectra 6 and 7, the intensity of $3p\sigma$ final cationic states is also quite strong, in fact as strong as $4p\sigma$ final cationic states. Following the relaxation model, the shake-down processes are expected to be negligible in these spectator decay processes. Therefore, the transition to $3p\sigma$ final cationic states is more likely due to the decay from the O $1s^{-1}$ ($^2\Sigma_u^-$) $3p'\sigma$ Rydberg state, which suggests that the resonance lines 6 and 7 in Fig. 1 ($h\nu$=541.80 and 541.97 eV) have not only $4p\sigma$ ($^4\Sigma_u^-$), but also $3p'\sigma$ ($^2\Sigma_u^-$) character. This has also already been parts of the assignments made recently by Kosugi and co-workers [13,19] for the resonance line 7, but since we

TABLE III. Energies, assignments (main components), and effective quantum numbers for the Rydberg states identified in the resonant Auger-electron spectrum recorded at $h\nu$=541.80 eV (cf. Figs. 2 and 3).

Line	KE (eV)	BE (eV)[a]	Transition	n^*
1	506.80	35.0	($^4\Sigma_u^-$) $4p\sigma\rightarrow$(W $^3\Delta_u$) $3p\sigma$	2.62
2	505.50	36.3	($^4\Sigma_u^-$) $4p\sigma\rightarrow$(B′ $^3\Sigma_u^-$+B $^3\Pi_g$) $3p\sigma$	2.69
3	503.20	38.6	($^4\Sigma_u^-$) $4p\sigma\rightarrow$(W $^3\Delta_u$) $4p\sigma$	3.56
4	502.10	39.7	($^4\Sigma_u^-$) $4p\sigma\rightarrow$(B′ $^3\Sigma_u^-$+B $^3\Pi_g$) $4p\sigma$	3.64
5	501.50	40.3	($^4\Sigma_u^-$) $4p\sigma\rightarrow$(W $^3\Delta_u$) $5p\sigma$	4.58
6	500.70	41.1	($^4\Sigma_u^-$) $4p\sigma\rightarrow$(W $^3\Delta_u$) $6p\sigma$	5.50
7	500.40	41.4	($^4\Sigma_u^-$) $4p\sigma\rightarrow$(B′ $^3\Sigma_u^-$+B $^3\Pi_g$) $5p\sigma$	4.76
8	497.50	44.3	($^4\Sigma_u^-$) $4p\sigma\rightarrow$(2 $^3\Pi_u$) $4p\sigma$	3.48
9	495.70	46.1	($^4\Sigma_u^-$) $4p\sigma\rightarrow$(2 $^3\Pi_u$) $5p\sigma$	4.49
10	494.40	47.4	($^4\Sigma_u^-$) $4p\sigma\rightarrow$(2 $^3\Sigma_g^-$) $4p\sigma$	3.64
11	492.90	48.9	($^4\Sigma_u^-$) $4p\sigma\rightarrow$(2 $^3\Sigma_g^-$) $5p\sigma$	4.58
12	492.20	49.6	($^4\Sigma_u^-$) $4p\sigma\rightarrow$(2 $^3\Sigma_g^-$) $6p\sigma$	5.35

[a]Of final state.

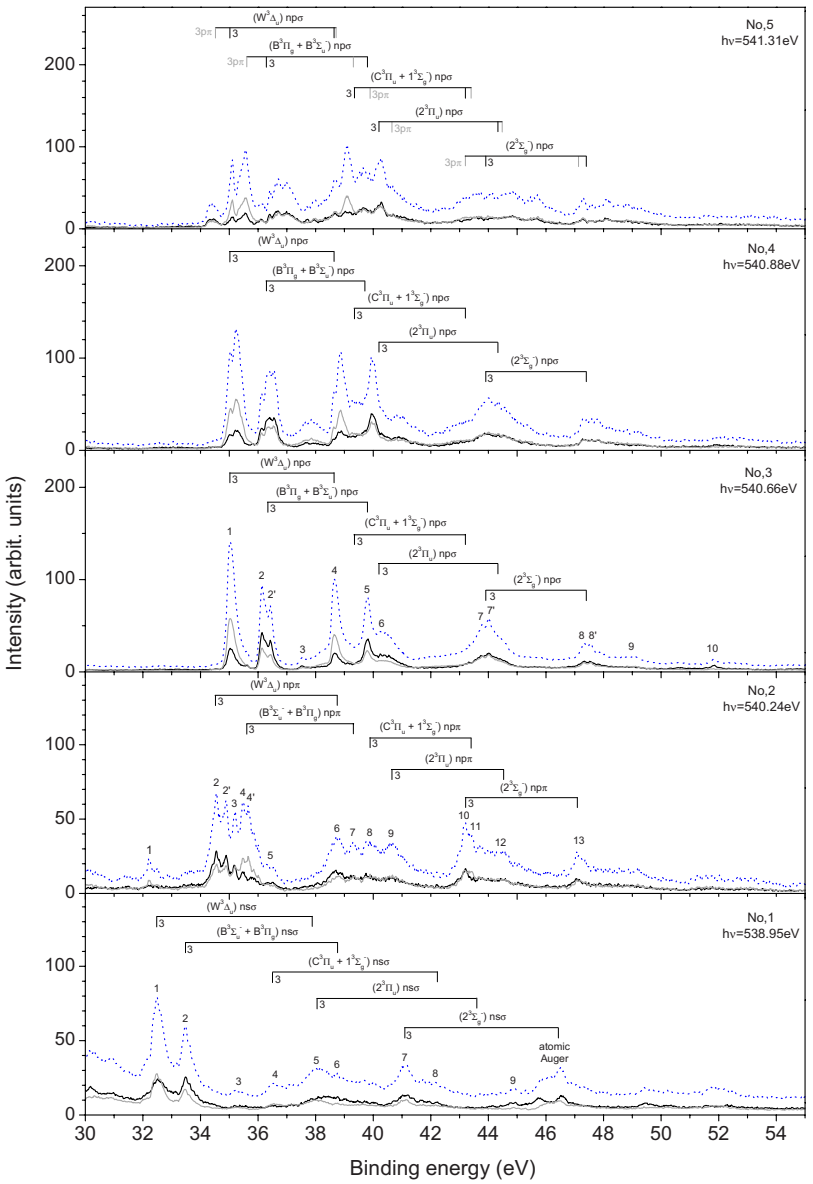

FIG. 4. (Color online) Normalized resonant Auger-electron spectra obtained for the photon energies 538.95, 540.24, 540.66, 540.88, and 541.31 eV, respectively. Spectra recorded at 0° and 90° relative to the electric field vector of the linear polarized synchrotron light are included, as well as the ones corrected for anisotropic electron emission (54.7°). Assignments of the various spectator Auger-electron final states in terms of Rydberg series in the cation converging towards the dicationic ionization limits are also included together with the principal quantum number n for some of the states. Line numbers, which are apostrophized, are tentatively assigned as vibrational excitations of the corresponding electronic states with nonapostrophized numbers (see also Tables IV–VI).

observe a substantial enhancement of the $3p\sigma$ final cationic states both at 541.80 and 541.97 eV photon energy (corresponding to peaks 6 and 7 of Fig. 1), we suggest to partially assign the resonance line 6 in Fig. 1 as the $v=0$ vibrational component and the line 7 as the $v=1$ vibrational component of the O $1s^{-1}$ $3p'\sigma$ ($^2\Sigma_u^-$) state, which coincide with the corresponding components of the O $1s^{-1}$ $4p\sigma$ ($^4\Sigma_u^-$) state, respectively (see, in particular, the middle panel of Fig. 1). Indeed, a similar assignment has already been proposed by Kosugi *et al.* in their original work [10]. It should be noted that the width of the resonance line 6 in Fig. 1 is apparently larger than the width of line 7, which could suggest that the $v=0$ components of the O $1s^{-1}$ $4p\sigma$ ($^4\Sigma_u^-$) and O $1s^{-1}$ $3p'\sigma$ ($^2\Sigma_u^-$) states do not perfectly coincide, but are slightly shifted relative to each other as marked in this figure.

Using this way of examining the resonant Auger-electron spectra on the grounds of existing assignments for the core-excited states, it is fairly straightforward to identify several ionic Rydberg series with consistent quantum defects, and vice versa, to use the resonant Auger-electron spectra for consistency tests of the assignments for the intermediate Rydberg states available from the literature.

Before we continue our discussion on the electron spectra recorded for even higher Rydberg excitations (i.e., on top of the resonance lines 8, 9, and 10 of Fig. 1), let us first turn our attention to the spectra measured on top of peaks 1–5 of Fig. 1, which are displayed in Fig. 4 together with assignments. In order to assign these electron spectra we could essentially adopt the assignment of the intermediate resonance states from Kosugi and co-workers [10,13,19], which we found generally consistent in this spectral region. For instance, all the features in the electron spectrum measured on top of peak 1 in Fig. 1 ($h\nu$=538.95 eV) which is, in a simplified picture [34], assigned to the O $1s^{-1}$ $3s\sigma$ ($^4\Sigma_u^-$) Rydberg state [10,13,19], are found to be explainable within the relaxation model in terms of mostly $ns\sigma$ ionic Rydberg series; we can also identify some $np\sigma$ contributions, though they are minor. In the Π-channel photoabsorption spectrum there is also a comparatively weak spectral band centered around 538.95 eV discernible, which is well in accordance with the

TABLE IV. Energies, assignments (main components), and effective quantum numbers for the Rydberg states identified in the resonant Auger-electron spectrum recorded at $h\nu$=538.95 eV (cf. Fig. 4).

Line	KE (eV)	BE (eV)[a]	Transition	n^*
1	506.45	32.5	$(^4\Sigma_u^-)\ 3s\sigma \rightarrow (\mathrm{W}\ ^3\Delta_u)\ 3s\sigma$	2.29
2	505.45	33.5	$(^4\Sigma_u^-)\ 3s\sigma \rightarrow (\mathrm{B}'\ ^3\Sigma_u^- + \mathrm{B}\ ^3\Pi_g)\ 3s\sigma$	2.30
3	503.65	35.3	$(^4\Sigma_u^-)\ 3s\sigma \rightarrow ?$	
4	502.45	36.5	$(^4\Sigma_u^-)\ 3s\sigma \rightarrow (\mathrm{C}\ ^3\Pi_u + 1\ ^3\Sigma_g)\ 3s\sigma$	2.21
5	500.85	38.1	$(^4\Sigma_u^-)\ 3s\sigma \rightarrow (2\ ^3\Pi_u)\ 3s\sigma$	2.26
6	500.15	38.8	$(^4\Sigma_u^-)\ 3s\sigma \rightarrow (\mathrm{B}'\ ^3\Sigma_u^- + \mathrm{B}\ ^3\Pi_g)\ 4s\sigma$	3.30
7	497.85	41.1	$(^4\Sigma_u^-)\ 3s\sigma \rightarrow (2\ ^3\Sigma_g^-)\ 3s\sigma$	2.29
8	496.75	42.2	$(^4\Sigma_u^-)\ 3s\sigma \rightarrow (\mathrm{C}\ ^3\Pi_u + 1\ ^3\Sigma_g)\ 4s\sigma$	3.17
9	494.05	44.9	$(^4\Sigma_u^-)\ 3s\sigma \rightarrow ?$	

[a]Of final state.

earlier measurements of Yagishita *et al.* [13] and which is likely to reflect a valence satellite state of Π symmetry. A more conclusive assignment of this spectral feature requires further experimental and theoretical investigations.

The features in the electron spectrum measured on top of the well-isolated resonance line 2 in Fig. 1 ($h\nu$ =540.24 eV) which is assigned to the O $1s^{-1}$ $3p\pi$ $(^4\Sigma_u^-)$ Rydberg state [10,13,19], can accordingly be explained in terms of overlapping $np\pi$ ionic Rydberg series as indicated in the figure. Moreover, the resonant Auger-electron spectra recorded on top of peaks 3 and 4 of Fig. 1 ($h\nu$=540.66 and 540.88 eV, respectively) are found to mainly reflect the response to vibrational excitations within the same intermediate Rydberg resonance state, i.e., the O $1s^{-1}$ $3p\sigma$ $(^4\Sigma_u^-)$ state [10,13,19], since the intensity ratios of the bands for the groups of different n in the spectator Auger-electron final states, as assigned here, are the same. In addition to that, as was readily found above for the resonant Auger-electron spectra 6 and 7 of Fig. 2 ($h\nu$=541.80 and 541.97 eV), this vibrational excitation causes line broadening and splitting in electron spectrum 4 ($h\nu$=540.88 eV) in comparison to electron spectrum 3 ($h\nu$=540.66 eV). By examining also the resonant Auger-electron spectrum measured on top of peak 5 of Fig. 1 ($h\nu$=541.31 eV) we noticed that we still clearly can see the same series of ionic Rydberg states as just identified in the electron spectra 3 and 4. However, this spectrum also contains additional contributions which most likely belong to $np\pi$ ionic Rydberg series as marked in the figure, being well in accord with the overlap of the v=3 vibrational level of the O $1s^{-1}$ $3p\sigma$ $(^4\Sigma_u^-)$ state and the v=1 level of the O $1s^{-1}$ $3p'\pi$ $(^2\Sigma_u^-)$ state as disentangled in the symmetry-resolved absorption curves of the middle and lower panels of Fig. 1 (cf.

TABLE V. Energies, assignments (main components), and effective quantum numbers for the Rydberg states identified in the resonant Auger-electron spectrum recorded at $h\nu$=540.24 eV (cf. Fig. 4). Line numbers, which are apostrophized, are tentatively assigned as vibrational excitations of the corresponding electronic states with nonapostrophized numbers.

Line	KE (eV)	BE (eV)[a]	Transition	n^*
1	508.04	32.2	$(^4\Sigma_u^-)\ 3p\pi \rightarrow ?$	
2	505.64	34.6	$(^4\Sigma_u^-)\ 3p\pi \rightarrow (\mathrm{W}\ ^3\Delta_u)\ 3p\pi$	2.56
2′	505.34	34.9	$(^4\Sigma_u^-)\ 3p\pi \rightarrow (\mathrm{W}\ ^3\Delta_u)\ 3p\pi$	2.61
3	505.04	35.2	$(^4\Sigma_u^-)\ 3p\pi \rightarrow ?$	
4	504.74	35.5	$(^4\Sigma_u^-)\ 3p\pi \rightarrow (\mathrm{B}'\ ^3\Sigma_u^- + \mathrm{B}\ ^3\Pi_g)\ 3p\pi$	2.56
4′	504.54	35.7	$(^4\Sigma_u^-)\ 3p\pi \rightarrow (\mathrm{B}'\ ^3\Sigma_u^- + \mathrm{B}\ ^3\Pi_g)\ 3p\pi$	2.59
5	503.84	36.4	$(^4\Sigma_u^-)\ 3p\pi \rightarrow ?$	
6	501.44	38.8	$(^4\Sigma_u^-)\ 3p\pi \rightarrow (\mathrm{W}\ ^3\Delta_u)\ 4p\pi$	3.64
7	500.94	39.3	$(^4\Sigma_u^-)\ 3p\pi \rightarrow (\mathrm{B}'\ ^3\Sigma_u^- + \mathrm{B}\ ^3\Pi_g)\ 4p\pi$	3.48
8	500.34	39.9	$(^4\Sigma_u^-)\ 3p\pi \rightarrow (\mathrm{C}\ ^3\Pi_u + 1\ ^3\Sigma_g)\ 3p\pi$	2.66
9	499.54	40.7	$(^4\Sigma_u^-)\ 3p\pi \rightarrow (2\ ^3\Pi_u)\ 3p\pi$	2.59
10	497.04	43.2	$(^4\Sigma_u^-)\ 3p\pi \rightarrow (2\ ^3\Sigma_g^-)\ 3p\pi$	2.56
11	496.84	43.4	$(^4\Sigma_u^-)\ 3p\pi \rightarrow (\mathrm{C}\ ^3\Pi_u + 1\ ^3\Sigma_g)\ 4p\pi$	3.60
12	495.74	44.5	$(^4\Sigma_u^-)\ 3p\pi \rightarrow (2\ ^3\Pi_u)\ 4p\pi$	3.56
13	493.14	47.1	$(^4\Sigma_u^-)\ 3p\pi \rightarrow (2\ ^3\Sigma_g^-)\ 4p\pi$	3.52

[a]Of final state.

TABLE VI. Energies, assignments (main components), and effective quantum numbers for the Rydberg states identified in the resonant Auger-electron spectrum recorded at $h\nu$=540.66 eV (cf. Fig. 4). Line numbers, which are apostrophized, are tentatively assigned as vibrational excitations of the corresponding electronic states with nonapostrophized numbers.

Line	KE (eV)	BE (eV)[a]	Transition	n^*
1	505.66	35.0	$(^4\Sigma_u^-)\ 3p\sigma \rightarrow (W\ ^3\Delta_u)\ 3p\sigma$	2.64
2	504.56	36.1	$(^4\Sigma_u^-)\ 3p\sigma \rightarrow (B'\ ^3\Sigma_u^- + B\ ^3\Pi_g)\ 3p\sigma$	2.66
2′	504.26	36.4	$(^4\Sigma_u^-)\ 3p\sigma \rightarrow (B'\ ^3\Sigma_u^- + B\ ^3\Pi_g)\ 3p\sigma$	2.71
3	503.16	37.5	$(^4\Sigma_u^-)\ 3p\sigma \rightarrow ?$	
4	502.06	38.6	$(^4\Sigma_u^-)\ 3p\sigma \rightarrow (W\ ^3\Delta_u)\ 4p\sigma$	3.60
5	500.86	39.8	$(^4\Sigma_u^-)\ 3p\sigma \rightarrow (B'\ ^3\Sigma_u^- + B\ ^3\Pi_g)\ 4p\sigma$	3.69
6	500.46	40.2	$(^4\Sigma_u^-)\ 3p\sigma \rightarrow (2\ ^3\Pi_u)\ 3p\sigma$	2.71
7	496.86	43.8	$(^4\Sigma_u^-)\ 3p\sigma \rightarrow (2\ ^3\Sigma_g^-)\ 3p\sigma$	2.71
7′	496.66	44.0	$(^4\Sigma_u^-)\ 3p\sigma \rightarrow (2\ ^3\Sigma_g^-)\ 3p\sigma$	2.75
8	493.26	47.4	$(^4\Sigma_u^-)\ 3p\sigma \rightarrow (2\ ^3\Sigma_g^-)\ 4p\sigma$	3.78
8′	493.06	47.6	$(^4\Sigma_u^-)\ 3p\sigma \rightarrow (2\ ^3\Sigma_g^-)\ 4p\sigma$	3.89

[a]Of final state.

corresponding energy position of line 5 in the upper panel of Fig. 1; see also Refs. [13,19]). The assignments for the resonant Auger-electron spectra 1, 2, and 3 are summarized in Tables IV–VI, respectively.

Please note that the confirmation for the resonance line structures 3–5 being part of the vibrational progression of the O $1s^{-1}\ 3p\sigma\ (^4\Sigma_u^-)$ state implies the manifestation of a strong underlying Rydberg-valence mixing through avoided curve crossings in the $^4\Sigma_u^-$ channel, as extensively discussed by Kosugi and co-workers [10,13,19]. Indeed, the Σ symmetry-resolved absorption curve (the middle panel of Fig. 1) clearly revealed vibrational levels of the O $1s^{-1}\ 3p\sigma\ (^4\Sigma_u^-)$ state up to at least v=5 ($h\nu$=541.58 eV), and a Franck-Condon analysis based on the assumption of underlying Morse potential curves results in the following vibrational constants for this electronic state: T_e=540.67 eV, w_e=0.242 eV, and $w_e x_e$=0.01 eV. It should also be noted in the present context, that a structure apparent at 541.62 eV photon energy in the Π symmetry-resolved absorption curve, previously assigned to the v=2 vibrational level of the O $1s^{-1}\ 3p'\pi\ (^2\Sigma_u^-)$ state, should probably be attributed to a different electronic state. We base this on the fact that the energy spacing between this

TABLE VII. Energies, assignments (main components), and effective quantum numbers for the Rydberg states identified in the resonant Auger-electron spectrum recorded at $h\nu$=542.26 eV (cf. Fig. 5).

Line	KE (eV)	BE (eV)[a]	Transition	n^*
1	506.66	35.6	$(^4\Sigma_u^-)\ 3d\sigma \rightarrow (W\ ^3\Delta_u)\ 3d\sigma$	2.75
2	505.66	36.6	$(^4\Sigma_u^-)\ 3d\sigma \rightarrow (B'\ ^3\Sigma_u^- + B\ ^3\Pi_g)\ 3d\sigma$	2.75
3	504.46	37.8	$(^4\Sigma_u^-)\ 3d\sigma \rightarrow ?$	
4	503.66	38.6	$(^4\Sigma_u^-)\ 3d\sigma \rightarrow (W\ ^3\Delta_u)\ 4p\sigma$	3.60
5	503.16	39.1	$(^4\Sigma_u^-)\ 3d\sigma \rightarrow (W\ ^3\Delta_u)\ 4d\sigma$	3.89
6	502.56	39.7	$(^4\Sigma_u^-)\ 3d\sigma \rightarrow (B'\ ^3\Sigma_u^- + B\ ^3\Pi_g)\ 4p\sigma$	3.64
7	502.06	40.2	$(^4\Sigma_u^-)\ 3d\sigma \rightarrow (B'\ ^3\Sigma_u^- + B\ ^3\Pi_g)\ 4d\sigma$	3.89
8	501.76	40.5	$(^4\Sigma_u^-)\ 3d\sigma \rightarrow (W\ ^3\Delta_u)\ 5d\sigma$	4.86
9	501.16	41.1	$(^4\Sigma_u^-)\ 3d\sigma \rightarrow (W\ ^3\Delta_u)\ 6p\sigma$	5.66
10	500.76	41.5	$(^4\Sigma_u^-)\ 3d\sigma \rightarrow (B'\ ^3\Sigma_u^- + B\ ^3\Pi_g)\ 5d\sigma$	4.86
11	500.36	41.9	$(^4\Sigma_u^-)\ 3d\sigma \rightarrow (B'\ ^3\Sigma_u^- + B\ ^3\Pi_g)\ 6p\sigma$	5.35
12	499.96	42.3	$(^4\Sigma_u^-)\ 3d\sigma \rightarrow (B'\ ^3\Sigma_u^- + B\ ^3\Pi_g)\ 7p\sigma$	6.02
13	496.76	45.5	$(^4\Sigma_u^-)\ 3d\sigma \rightarrow (C\ ^3\Pi_u + 1\ ^3\Sigma_g)\ 6p\sigma$	5.09
14	495.36	46.9	$(^4\Sigma_u^-)\ 3d\sigma \rightarrow (2\ ^3\Pi_u)\ 6p\sigma$	5.35
15	493.36	48.9	$(^4\Sigma_u^-)\ 3d\sigma \rightarrow (2\ ^3\Sigma_g^-)\ 5p\sigma$	4.58
16	493.16	49.1	$(^4\Sigma_u^-)\ 3d\sigma \rightarrow (2\ ^3\Sigma_g^-)\ 5d\sigma$	4.76
17	492.66	49.6	$(^4\Sigma_u^-)\ 3d\sigma \rightarrow (2\ ^3\Sigma_g^-)\ 6p\sigma$	5.35
18	492.16	50.1	$(^4\Sigma_u^-)\ 3d\sigma \rightarrow (2\ ^3\Sigma_g^-)\ 7p\sigma$	6.40

[a]Of final state.

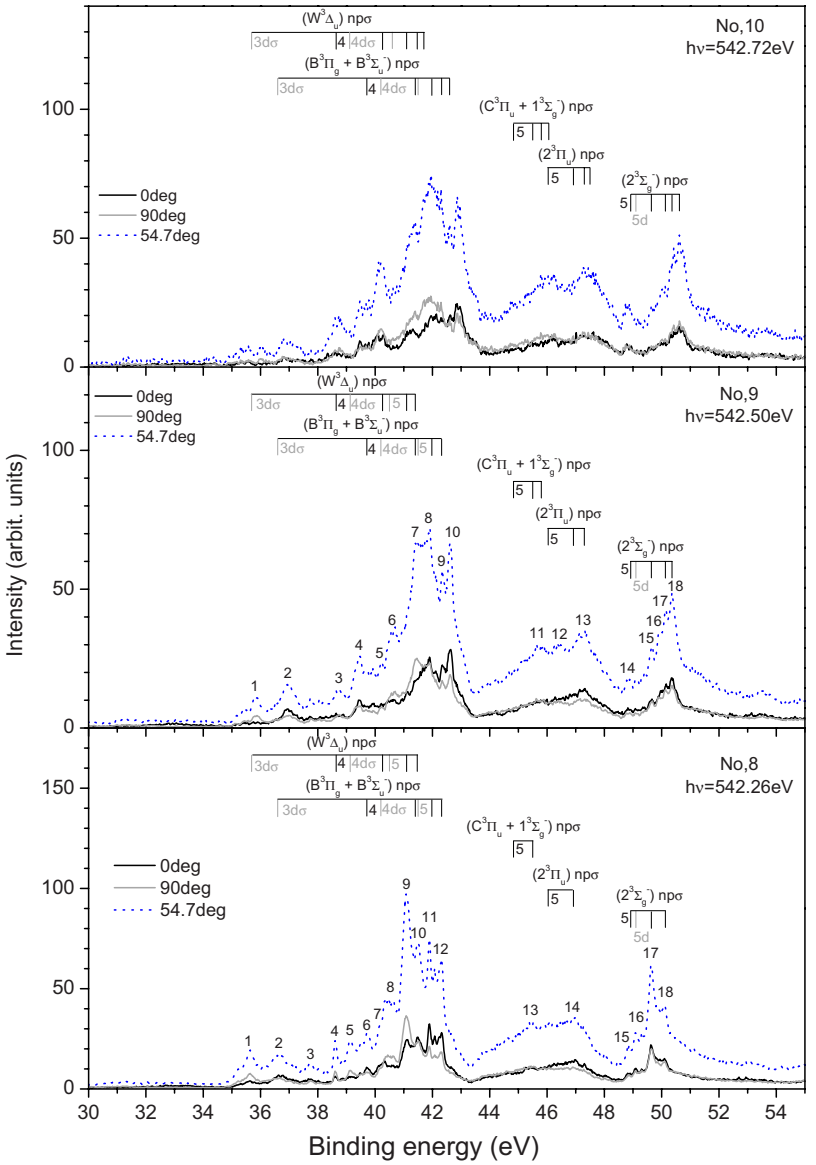

FIG. 5. (Color online) Normalized resonant Auger-electron spectra obtained for the photon energies 542.26 eV (lower panel; cf. upper panel of Fig. 2), 542.50 eV (middle panel), and 542.72 eV (upper panel), respectively. Spectra recorded at 0° and 90° relative to the electric field vector of the linear polarized synchrotron light are included, as well as the ones corrected for anisotropic electron emission (54.7°). Assignments of the various spectator-Auger-electron final states in terms of Rydberg series in the cation converging towards the dicationic ionization limits are also included together with the principal quantum number n for some of the states (see also Tables VII and VIII).

line and its nearest (low-energy) neighbor is larger than the spacing between the two nearest neighboring lines on the low photon energy side. A suitable candidate for this state, with respect to the most likely quantum defect, could be the O $1s^{-1}$ $3d\pi$ ($^4\Sigma_u^-$) Rydberg state. Accordingly, we also suggest alternative assignments for some of the resonance features resolved at higher photon energies in the Π channel, as marked in the lower panel of Fig. 1. All the assignments of the core-excited states are summarized in Tables I and II.

Let us now discuss the resonant Auger-electron spectra recorded for excitations on top of the resonance lines 8, 9, and 10 of Fig. 1 ($h\nu$=542.26, 542.50, and 542.72 eV, respectively), which are displayed in Fig. 5. As a starting point, we should take a closer look at the symmetry-resolved photoabsorption spectra of Fig. 1. As we can see, the dominat intermediate electronic states in this fairly complex spectral region can be expected to be primarily of Σ symmetry according to the relative strengths of the two channels in this photon energy region. Looking at the well-resolved group in the Σ channel (lines 8–10), it appears plausible that these lines constitute a vibrational progression of a single electronic state. According to previous investigations [10,13,19], however, line 8 is attributed to the O $1s^{-1}$ $5p\sigma$ ($^4\Sigma_u^-$) Rydberg state, line 9 to the O $1s^{-1}$ $6p\sigma$ ($^4\Sigma_u^-$) Rydberg state, and line 10 was originally suggested to be the O $1s^{-1}$ $7p\sigma$ ($^4\Sigma_u^-$) Rydberg state [10], and has recently been altered to the O $1s^{-1}$ $4p'\sigma$ ($^2\Sigma_u^-$) Rydberg state [13,19]. By looking at the effective quantum numbers n^* of the lines 8–10 in Fig. 1, however, we noticed that the quantum defects $\delta=n-n^*$ vary substantially and even take unrealistically large values in comparison to lines 3 and 6, if all these lines were assigned to members of the same Rydberg series, i.e., the $np\sigma$ ($^4\Sigma_u^-$) series. For instance, in assigning lines 8–10 to the $5p\sigma$ ($^4\Sigma_u^-$), $6p\sigma$ ($^4\Sigma_u^-$), and $7p\sigma$ ($^4\Sigma_u^-$) Rydberg states, respectively, one receives quantum defects δ=1.55, 2.13, and 2.49, respectively.

Hence, using the effective quantum numbers as a guide, one may plausibly assign lines 8 and 9 to the $3d\sigma$ and $5p\sigma$ ($^4\Sigma_u^-$) Rydberg states, and line 10 to the $4d\sigma$ ($^4\Sigma_u^-$) Rydberg state, respectively (cf. Table I). According to the rule of

TABLE VIII. Energies, assignments (main components), and effective quantum numbers for the Rydberg states identified in the resonant Auger-electron spectrum recorded at $h\nu$=542.50 eV (cf. Fig. 5).

Line	KE (eV)	BE (eV)[a]	Transition	n^*
1	506.70	35.8	$(^4\Sigma_u^-)\ 5p\sigma \rightarrow (W\ ^3\Delta_u)\ 3d\sigma$	2.78
2	505.60	36.9	$(^4\Sigma_u^-)\ 5p\sigma \rightarrow (B'\ ^3\Sigma_u^- + B\ ^3\Pi_g)\ 3d\sigma$	2.81
3	503.80	38.7	$(^4\Sigma_u^-)\ 5p\sigma \rightarrow (W\ ^3\Delta_u)\ 4p\sigma$	3.64
4	503.10	39.4	$(^4\Sigma_u^-)\ 5p\sigma \rightarrow ?$	
5	502.30	40.2	$(^4\Sigma_u^-)\ 5p\sigma \rightarrow (W\ ^3\Delta_u)\ 5p\sigma$	4.57
6	501.90	40.6	$(^4\Sigma_u^-)\ 5p\sigma \rightarrow (W\ ^3\Delta_u)\ 5d\sigma$	4.97
7	501.10	41.4	$(^4\Sigma_u^-)\ 5p\sigma \rightarrow (W\ ^3\Delta_u)\ 7p\sigma$	6.23
8	500.60	41.9	$(^4\Sigma_u^-)\ 5p\sigma \rightarrow (B'\ ^3\Sigma_u^- + B\ ^3\Pi_g)\ 6p\sigma$	5.35
9	500.20	42.3	$(^4\Sigma_u^-)\ 5p\sigma \rightarrow (B'\ ^3\Sigma_u^- + B\ ^3\Pi_g)\ 7p\sigma$	6.02
10	499.90	42.6	$(^4\Sigma_u^-)\ 5p\sigma \rightarrow (B'\ ^3\Sigma_u^- + B\ ^3\Pi_g)\ 8p\sigma$	6.73
11	496.80	45.7	$(^4\Sigma_u^-)\ 5p\sigma \rightarrow (C\ ^3\Pi_u + 1\ ^3\Sigma_g)\ 6s\sigma$	5.35
12	496.10	46.4	$(^4\Sigma_u^-)\ 5p\sigma \rightarrow ?$	
13	495.20	47.3	$(^4\Sigma_u^-)\ 5p\sigma \rightarrow (2\ ^3\Pi_u)\ n\sigma$	6.02
14	493.70	48.8	$(^4\Sigma_u^-)\ 5p\sigma \rightarrow (2\ ^3\Sigma_g^-)\ n\sigma$	4.49
15	492.80	49.7	$(^4\Sigma_u^-)\ 5p\sigma \rightarrow (2\ ^3\Sigma_g^-)\ n\sigma$	5.50
16	492.50	50.0	$(^4\Sigma_u^-)\ 5p\sigma \rightarrow (2\ ^3\Sigma_g^-)\ n\sigma$	6.02
17	492.40	50.1	$(^4\Sigma_u^-)\ 5p\sigma \rightarrow (2\ ^3\Sigma_g^-)\ n\sigma$	6.23
18	492.10	50.4	$(^4\Sigma_u^-)\ 5p\sigma \rightarrow (2\ ^3\Sigma_g^-)\ n\sigma$	7.03

[a]Of final state.

thumb for quantum defects, values for *nd* Rydberg series are usually 0.1–0.2. Thus, one may consider that it would be more reasonable to assign lines 6 and 9 to $3d\sigma$ and $4d\sigma$ with quantum defects of $\approx$0.1, while assigning lines 8 and 10 to $4p\sigma$ and $5p\sigma$ with quantum defects of $\approx$0.5. However, as we have already discussed, the assignment of line 6 to $(^4\Sigma_u^-)\ 4p\sigma$ [with an additional accidental overlap of $(^2\Sigma_u^-)\ 3p'\sigma$] was verified by the resonant Auger-electron spectra recorded on top of peaks 6 and 7 [23]. We note that line 9 may also have a contribution from the overlap with vibrational excitation of line 8.

Based on the assignment of the resonance line 8 to $3d\sigma$, we tried to assign accordingly the Auger-electron final Rydberg states in the top panel of Fig. 2 and the bottom panel of Fig. 5, using the spectator-shake relaxation model. The energies of the Auger-electron final states and their assignments are summarized in Table VII. As can be seen in the table, the introduction of the $3d\sigma$ intermediate state level of line 8 gives assignments for the spectator Auger-electron final states for consistency with this model. We note, however, that $np\sigma$ Auger-electron final states are also populated. This suggests mixing of the *p* and *d* characters to be present in several of the core-excited Rydberg states.

The energies of the final states for the resonant Auger decay from line 9 and their assignments are summarized in Table VIII. Apparently we see both *np* and *nd* Rydberg series, indicating the *p*-*d* mixing. Some of the lines, such as lines 1, 2, and 4 should be identified as the vibrational excitation of the same electronic states for lines 1, 2, and 5 in Table VIII, illustrating that line 9 has a contribution from the vibrational excitation of line 8. Higher Rydberg members of the Auger-electron final states, however, indicates that the main component of line 9 has larger *np* configuration than line 8.

Furthermore, the absorption line resolved at 542.89 eV photon energy (s17 in Fig. 1), located next to line 10, fits energetically well to the $3d'\sigma$ $(^2\Sigma_u^-)$ Rydberg state, with the quantum defect of $\sim$0.1 (cf. Table I). The next line at 543.18 eV photon energy (s18 in Fig. 1) may well fit to $4p'$ $(^2\Sigma_u^-)$, with a quantum defect of $\sim$0.7. More profound theoretical work is needed in order to confirm these detailed assignments.

IV. SUMMARY

A series of resonant Auger-electron spectra, measured at ten selected photon energies across the O $1s \rightarrow$ Rydberg resonances in O_2 between 538.95 and 542.72 eV has been presented and analyzed. The analysis was based on the spectator-electron shake relaxation model originally introduced for atomic resonant Auger-electron spectra and on assignments for the core-excited resonances as, to a large extent, available from the literature. In this way, many of the observed spectator-Auger-electron final states could be assigned in terms of cationic Rydberg series. Vice versa, the resonant Auger-electron spectra were used for consistency tests of the literature assignments available for the core-excited intermediate Rydberg states. For some of the latter ones, in particular, in the high photon energy region of the absorption spectrum, alternative assignments are proposed, which are awaiting theoretical support.

ACKNOWLEDGMENTS

The experiments were carried out with the approval of

JASRI. We are grateful to the staff of SPring-8 for assistance during the measurements. The work was supported in part by Grants-in-aid for Scientific Research from the Japan Society for the Promotion of Science (JSPS), the Swedish Research Council (VR), the Foundation for Strategic Research (SSF), and by the Swedish Foundation for International Cooperation in Research and Higher Education STINT. R.F. acknowledges Tohoku University for hospitality and financial support during his stay there.

[1] M. N. Piancastelli, J. Electron Spectrosc. Relat. Phenom. **107**, 1 (2000).
[2] S. L. Sorensen and S. Svensson, J. Electron Spectrosc. Relat. Phenom. **114-116**, 1 (2001).
[3] J. D. Bozek, S. E. Canton, E. Kukk, and N. Berrah, Chem. Phys. **289**, 149 (2003).
[4] K. Ueda, J. Phys. B **36**, R1 (2003).
[5] K. Ueda, J. Phys. Soc. Jpn. **75**, 032001 (2006).
[6] A. P. Hitchcock and C. R. Brion, J. Phys. Soc. Jpn. **18**, 1 (1980).
[7] W. Wurth, J. Stöhr, P. Feulner, X. Pan, K. R. Bauchspiess, Y. Baba, E. Hudel, G. Rocker, and D. Menzel, Phys. Rev. Lett. **65**, 2426 (1990).
[8] M. W. Ruckman, J. Chen, S. L. Qiu, P. Kuiper, M. Strongin, and B. I. Dunlap, Phys. Rev. Lett. **67**, 2533 (1991).
[9] Y. Ma, C. T. Chen, G. Meigs, K. Randall, and F. Sette, Phys. Rev. A **44**, 1848 (1991).
[10] N. Kosugi, E. Shigemasa, and A. Yagishita, Chem. Phys. Lett. **190**, 481 (1992).
[11] M. Neeb, J.-E. Rubensson, M. Biermann, and W. Eberhardt, Phys. Rev. Lett. **71**, 3091 (1993).
[12] P. Kuiper and B. I. Dunlap, J. Chem. Phys. **100**, 4087 (1994).
[13] A. Yagishita, E. Shigemasa, and N. Kosugi, Phys. Rev. Lett. **72**, 3961 (1994).
[14] H. Ågren, L. Yang, V. Caravetta, and L. G. M. Pettersson, Chem. Phys. Lett. **259**, 21 (1996).
[15] A. Kivimäki, B. Kempgens, M.-N. Piancastelli, M. Neeb, K. Maier, A. Rüdel, U. Hergenhahn, and A. M. Bradshaw, J. Electron Spectrosc. Relat. Phenom. **93**, 81 (1998).
[16] M.-N. Piancastelli, A. Kivimäki, V. Carravetta, I. Cacelli, R. Cimiraglia, C. Angeli, H. Wang, M. Coreno, M. de Simone, G. Turri, and K. C. Prince, Phys. Rev. Lett. **88**, 243002 (2002).
[17] N. Kosugi, Chem. Phys. **289**, 117 (2003).
[18] I. Hjelte, O. Björneholm, V. Caravetta, C. Angeli, R. Cimiraglia, K. Wiesner, S. Svensson, and M.-N. Piancastelli, J. Chem. Phys. **123**, 064314 (2005).
[19] J. Adachi, N. Kosugi, and A. Yagishita, J. Phys. B **38**, R127 (2005).
[20] S. Sorensen, K. J. Borve, R. Feifel, A. de Fanis, and K. Ueda, J. Phys. B **41**, 095101 (2008).
[21] M. Coreno, M. de Simone, K. C. Prince, R. Richter, M. Vondraćek, L. Avaldi, and R. Camilloni, Chem. Phys. Lett. **306**, 269 (1999).
[22] M. Larsson, P. Baltzer, S. Svensson, B. Wannberg, N. Mårtensson, A. Naves de Brito, N. Corriea, M. P. Keane, M. Carlsson-Göthe, and L. Karlsson, J. Phys. B **23**, 1175 (1990).
[23] S. L. Sorensen, T. Tanaka, R. Feifel, J. H. D. Eland, M. Kitajima, H. Tanaka, R. Sankari, A. De Fanis, M.-N. Piancastelli, L. Karlsson, and K. Ueda, Chem. Phys. Lett. **398**, 168 (2004).
[24] K. Ueda, J. B. West, N. M. Kabachnik, Y. Sato, K. J. Ross, H. J. Beyer, H. Hamdy, and H. Kleinpoppen, Phys. Rev. A **54**, 490 (1996).
[25] H. Ohashi, E. Ishiguro, Y. Tamenori, H. Kishimoto, M. Tanaka, M. Irie, T. Tanaka, and T. Ishikawa, Nucl. Instrum. Methods Phys. Res. A **467-468**, 529 (2001).
[26] H. Ohashi, E. Ishiguro, Y. Tamenori, H. Okumura, A. Hiraya, H. Yoshida, Y. Senba, K. Okada, N. Saito, I. H. Suzuki, K. Ueda, T. Ibuki, S. Nagaoka, I. Koyano, and T. Ishikawa, Nucl. Instrum. Methods Phys. Res. A **467-468**, 533 (2001).
[27] T. Tanaka and H. Kitamura, Nucl. Instrum. Methods Phys. Res. A **364**, 368 (1995).
[28] T. Tanaka and H. Kitamura, J. Synchrotron Radiat. **3**, 47 (1996).
[29] Y. Shimizu, H. Ohashi, Y. Tamenori, Y. Muramatsu, H. Yoshida, K. Okada, N. Saito, H. Tanaka, I. Koyano, S. Shin, and K. Ueda, J. Electron Spectrosc. Relat. Phenom. **114-116**, 63 (2001).
[30] H. Yoshida, Y. Senba, M. Morita, T. Goya, A. De Fanis, N. Saito, K. Ueda, Y. Tamenori, and H. Ohashi, in *Synchrotron Radiation Instrumentation: 8th International Conference on Synchrotron Radiation Instrumentation*, edited by T. Warwick, J. Arthur, H. A. Padmore, and J. Stöhr, AIP Conf. Proc. No. 705 (AIP, Melville, NY, 2004), p. 267.
[31] I. Koyano, M. Okuyama, E. Ishiguro, A. Hiraya, H. Ohashi, T. Kanashima, K. Ueda, I. H. Suzuki, and T. Ibuki, J. Synchrotron Radiat. **5**, 545 (1998).
[32] N. Saito, K. Ueda, M. Simon, K. Okada, Y. Shimizu, H. Chiba, Y. Senba, H. Okumura, H. Ohashi, Y. Tamenori, S. Nagaoka, A. Hiraya, H. Yoshida, E. Ishiguro, T. Ibuki, I. H. Suzuki, and I. Koyano, Phys. Rev. A **62**, 042503 (2000).
[33] P. Baltzer, B. Wannberg, L. Karlsson, M. Carlsson Göthe, and M. Larsson, Phys. Rev. A **45**, 4374 (1992).
[34] R. Feifel, Y. Velkov, V. Caravetta, C. Angeli, R. Cimiraglia, P. Salek, F. Gelmukhanov, S. L. Sorensen, M. N. Piancastelli, A. De Fanis, K. Okada, M. Kitajima, T. Tanaka, H. Tanaka, and K. Ueda, J. Chem. Phys. **128**, 064304 (2008).
[35] R. Manne and T. Åberg, Chem. Phys. Lett. **7**, 282 (1970).